Nigerian Journal of Applied Physics (NJAP)
ISSN Print: 3115-5871
ISSN Online: 3115-588X
DOI: https://doi.org/10.62292/njap-v2i2-2026-71
Volume 2(2), June 2026

Detection and Characterization of Exoplanets Using Transit Photometry

[1]Yakubu Mu'allim, *[2]Vwavware Jude Oruaode, [3]Ojobeagu Austin Okechukwu and [2]Ohwofosirai Adrian

[1]Department of Industrial Physics, Enugu State University of Science and Technology, Enugu, Nigeria
[2]Department of Physics, Dennis Osadebay University, Asaba, Delta State, Nigeria
[3]Department of Industrial and Medical Physics, David Umahi Federal University of Health Sciences, Uburu, Ebonyi State, Nigeria.

*Corresponding author's email: oruaode.vwavware@dou.edu.ng

ABSTRACT

Transit photometry has established itself as one of the most powerful and versatile techniques in exoplanet science, driving the discovery of thousands of planets and enabling quantitative studies of their physical properties. Completeness-corrected analyses of Kepler photometry demonstrate that small exoplanets (≈1–4 R⊕) are common around FGKM stars across a wide range of orbital periods. Advances in detection methodology, including transit least-squares searches and machine-learning–based validation frameworks, have significantly improved sensitivity to shallow transits and reduced false-positive contamination. Beyond demographics, transit photometry has become central to atmospheric characterization through transmission spectroscopy with facilities such as the James Webb Space Telescope (JWST). This paper discusses the methodological foundations of transit photometry, including light-curve extraction, transit detection, modelling, and validation. Key scientific outcomes from major surveys, particularly Kepler and TESS, are highlighted, including planet occurrence rates, multi-planet system architectures, and the discovery of the planetary "radius valley," which provides evidence for atmospheric mass-loss processes in small planets. The role of transit timing variations and joint analyses with radial-velocity data in constraining planetary masses and bulk compositions is also examined. Current limitations, notably stellar activity and observational biases, are critically assessed. Transit photometry will remain central to exoplanet discovery and atmospheric studies in the era of next-generation observatories.

Keywords:
Exoplanets,
Transit photometry,
Light Curves,
TESS,
Kepler,
Planetary radii.

INTRODUCTION

The discovery of exoplanets has transformed modern astrophysics by revealing the diversity of planetary systems beyond the Solar System (Perryman, 2012). Early exoplanet searches relied primarily on indirect detection methods such as radial velocity, astrometry, and transit photometry, which infer the presence of planets through their effects on host stars rather than through direct imaging (Perryman, 2012). The first confirmed detections of exoplanets orbiting pulsars, followed by the discovery of 51 Pegasi b around a Sun-like star in 1995, established the radial velocity method as the first successful technique for exoplanet detection (Cassan, 2021). Improvements in spectroscopic precision and long-term monitoring subsequently enabled the discovery of lower-mass planets and more complex planetary systems (Yang, 2024).

Transit photometry later emerged as the most productive exoplanet detection technique following the success of dedicated space missions such as Kepler and TESS (Deeg and Alonso, 2018). The method detects periodic decreases in stellar brightness when a planet passes in front of its host star along the observer's line of sight. The transit depth is approximately proportional to $(R_p/R_*)^2$, where (R_p) and (R_*) represent the planetary and stellar radii, respectively, enabling direct measurements of planetary size from light curves (Deeg & Alonso, 2018). Analytic transit models developed by Mandel & Agol (2002) provided the theoretical framework for accurate transit fitting and parameter extraction. In addition to planetary radii, transit duration, shape, and timing can constrain orbital inclination, period, and eccentricity, particularly when combined with radial velocity measurements (Winn, 2007).

The Kepler mission revolutionized exoplanet science by continuously monitoring over 150,000 stars with unprecedented photometric precision, leading to the discovery of thousands of confirmed and candidate exoplanets (Bryson et al., 2020). Statistical analyses of Kepler data revealed that small planets are common around FGKM stars and identified important demographic features such as the planetary "radius valley," a deficit of planets near ~1.8 $R_\oplus$ that is interpreted as evidence for atmospheric mass-loss processes (Fulton et al., 2017; Van Eylen et al., 2018). These discoveries significantly advanced understanding of planetary formation and evolution. The Transiting Exoplanet Survey Satellite (TESS), launched in 2018, expanded transit surveys to nearly the entire sky, focusing primarily on bright nearby stars suitable for follow-up observations (Barclay et al., 2018). TESS observations facilitate atmospheric characterization, radial velocity confirmation, and asteroseismic studies of host stars, improving measurements of stellar and planetary properties (Lund et al., 2017). In parallel, advances in automated data processing, machine-learning classification, and transit validation frameworks have improved sensitivity to shallow transit signals and reduced false-positive contamination in large photometric datasets (Armstrong et al., 2020; Valizadegan et al., 2021).

Transit photometry has also become a major tool for atmospheric characterization through transmission spectroscopy. Observations with the James Webb Space Telescope (JWST) have enabled high-precision detections of molecular species such as CO_2, H_2O, SO_2, and CH_4 in exoplanet atmospheres, providing insights into atmospheric chemistry, metallicity, and cloud properties (Alderson et al., 2023). These advances have strengthened the role of transit photometry not only in exoplanet detection but also in the broader study of planetary composition, atmospheric evolution, and potential habitability. This paper examines the principles, methodologies, and scientific applications of transit photometry in exoplanet detection and characterization. Particular emphasis is placed on Kepler and TESS discoveries, detection and validation techniques, occurrence-rate studies, the planetary radius valley, transit timing variations, and recent progress in atmospheric characterization with JWST. Current observational limitations and future prospects for next-generation missions are also discussed.

MATERIALS AND METHODS

Principles of Transit Photometry

Transit photometry is one of the most widely used methods for detecting and characterizing exoplanets. It is based on measuring the small decrease in stellar brightness that occurs when a planet passes in front of its host star along the observer's line of sight. The resulting transit light curve encodes key information about the planet's physical and orbital properties, including its size, orbit, and atmospheric effects (Volker, 2010; Seager & Mallén-Ornelas, 2003).

The geometry of a transit event depends on the orbital configuration of the planet relative to the observer. As the planet crosses the stellar disk, it follows a path determined by the orbital inclination. The main transit parameters include the orbital period (P), planet-to-star radius ratio ($R_p/R_\star$), orbital inclination (i), and impact parameter (b), which describes the sky-projected distance between the center of the stellar disk and the transit chord in units of stellar radius. The shape of the transit light curve is also strongly affected by stellar limb darkening, where the stellar surface appears brighter at the center than near the edge (Claret, 2000). The orbital structure is further described by the semi-major axis (a) and eccentricity (e), which control orbital separation and variations in orbital velocity. Planets in circular orbits generally produce symmetric light curves with consistent transit durations, whereas eccentric orbits can introduce asymmetries in timing and duration due to variations in orbital speed (Seager & Mallén-Ornelas, 2003). Transit probability is the likelihood that a planet's orbital plane is aligned such that it passes in front of its host star from the observer's perspective. This probability increases for planets closer to their host stars, since alignment requirements are less restrictive. For circular orbits, the transit probability is approximately:

$$P_{transit} \approx \frac{R_\star + R_p}{a}$$

Where (R_*) is the stellar radius, (R_p) is the planetary radius, and (a) is the orbital semi-major axis (Volker, 2010). For eccentric orbits, the probability becomes:

$$P_{transit} \approx \frac{R_\star + R_p}{a}, \frac{1+e\,sinw}{1-e^2}$$

Where (e) is the orbital eccentricity and ω is the argument of periastron (Barnes, 2007). Orbital inclination is defined as the angle between the orbital plane of the planet and the plane of the sky. An inclination of (90^0) corresponds to a perfectly edge-on configuration that produces the most favorable geometry for a transit. As inclination deviates from this value, the transit chord moves away from the stellar center, reducing both the transit probability and observed transit depth (Volker, 2010). The impact parameter is given by:

$$b = \frac{a^{Cosi}}{R_\star}$$

For circular orbits, where (i) is the orbital inclination. Low values of (b) correspond to central transits, while higher values indicate grazing transits with shorter durations and shallower depths (Seager & Mallén-Ornelas, 2003). The observed transit profile is also influenced by stellar limb darkening and stellar activity such as star spots and plages, which can distort the light curve and bias parameter estimation if not properly modelled. High-precision photometry and careful modelling are therefore

required to accurately recover planetary radii and orbital properties (Volker, 2010).

Joint Radial Velocity and Transit Analysis

Transit photometry provides precise measurements of planetary radius and orbital period but does not directly measure planetary mass. Radial velocity (RV) observations complement transit data by detecting Doppler shifts in stellar spectra caused by the gravitational influence of orbiting planets. The combination of transit and RV measurements enables the determination of planetary bulk density, which is essential for constraining composition and internal structure (Butler et al., 2006).

Joint transit–RV analysis is particularly important for distinguishing between rocky planets and volatile-rich sub-Neptunes or gas giants. Accurate mass and radius measurements also enable studies of planetary structure, atmospheric escape, and formation pathways. Empirical mass–radius relations derived from such combined datasets provide important constraints on planetary diversity (Weiss & Marcy, 2014). In multi-planet systems, radial velocity data can also be combined with transit timing variations (TTVs) to improve constraints on planetary masses and orbital dynamics. These combined methods are now central to modern exoplanet characterization and system architecture studies (Agol & Fabrycky, 2018).

Data Acquisition and Surveys

The data acquisition for exoplanet detection through transit photometry predominantly involves space-based missions such as Kepler, K2, TESS, and the forthcoming PLATO, alongside ground-based surveys like HATNet, WASP, and NGTS. The Kepler mission was revolutionary in exoplanet discovery by monitoring a fixed stellar field over nearly a decade with unprecedented photometric precision, leading to thousands of candidate and confirmed exoplanets detected via their transit signals (Babu, 2018). After its reaction wheel failures, the mission evolved into K2, which observed multiple ecliptic plane fields over ~75-day campaigns. K2 retained high photometric quality sufficient for transit detection, including single-transit events, enabling detection of planets with periods longer than the campaign duration (Osborn *et al*., 2015). The Transiting Exoplanet Survey Satellite (TESS), launched in 2018, expanded sky coverage by surveying nearly the entire sky in 27-day sectors, focusing on bright nearby stars, providing 2-minute cadence photometry for pre-selected targets and 30-minute full-frame images. TESS optimizes detection of small planets across diverse stellar populations (Burt and Barclay, 2017; Jiang *et al*., 2019). Its photometric data enables comprehensive planet detection and follow-up, facilitating demographic studies (Barclay *et al*., 2018; Brown & Latham, 2008). Robotic telescope networks have expanded the capability of ground-based transit surveys (Vwavware *et al*., 2025). The Next Generation Transit Survey (NGTS) operates at ESO Paranal Observatory with multiple 20cm telescopes achieving photometric precision sufficient to detect Neptune-sized and subNeptune planets around bright stars, also aiding in ground-based follow-up for TESS and PLATO candidates (Burleigh, 2017). Together, the synergy of these space- and ground-based photometric surveys enables wide sky coverage, high photometric precision, and diverse temporal baselines, making transit photometry a leading and effective method for exoplanet detection and characterization.

Data Reduction and Light Curve Extraction

Data reduction and light curve extraction in astronomical photometry involve several critical steps to convert raw observational data into precise and reliable stellar brightness measurements. Photometric calibration is the initial process that corrects raw flux measurements for instrumental response and atmospheric effects to derive accurate, standardized magnitudes. This calibration typically utilizes observations of standard stars or fields to apply zero-point adjustments and corrects for atmospheric extinction, ensuring uniformity and comparability of photometry across different observing conditions and instruments (Mohr *et al*., 2012). Detrending techniques are applied to time-series photometry to remove systematic trends arising from instrumental instabilities, atmospheric variations, or spacecraft effects. Using methods like polynomial fitting, splines, or algorithms such as the SysRem or Trend Filtering Algorithm (TFA), correlated noise sources are modelled and subtracted to enhance the astrophysical signal. Stellar flares can introduce noise in light curves, complicating transit detection (Yakubu *et al*., 2023). Multi-aperture photometry combined with spatio-temporal detrending has been shown to recover a higher fraction of usable data and improve light curve precision significantly (Irwin *et al*., 2007).

Transit Detection and Validation

Transit detection and validation rely on advanced algorithms, statistical analyses, and follow-up tools to identify and confirm exoplanet signals amidst noise and false positives. Period-search algorithms such as the Box Least Squares (BLS) method have long been the standard tool for detecting periodic transit signals characterized by box-shaped dips in stellar light curves. More recently, the Transit Least Squares (TLS) algorithm has been developed as a successor to BLS. TLS improves sensitivity, especially for smaller planets, by modelling more realistic transit shapes and enhancing detection efficiency. For example, TLS successfully detected an Earth-sized planet in the K2-32 system that was missed by BLS due to its lower detection efficiency in sub-

optimally detrended data (Heller et al., 2019). While BLS remains the standard for periodic box-shaped transit searches, TLS improves sensitivity to smaller planets and non-ideal detrending by modelling realistic transit shapes (Heller et al., 2019). GPU-accelerated pipelines such as CETRA significantly reduce computation time for large datasets, enabling rapid searches across extended parameter spaces. Machine-learning approaches, including transformer-based FFI searches and classifiers like ExoMiner++, offer high recall and precision but require careful training to avoid false positives from stellar variability or instrumental noise. In general, TLS and GPU-accelerated methods provide better sensitivity to shallow transits and single-events, while ML frameworks excel in automated vetting and candidate ranking. Detection thresholds and biases inherent in these algorithms affect the sensitivity and false positive rates. The signal detection efficiency metric is often used to assess candidate significance, but thresholds can exclude planets with low signal-to-noise or sparse transits.

The analytic transit model developed by Mandel & Agol (2002) provides exact formulae for planetary transit light curves, incorporating stellar limb-darkening effects and enabling precise inference of transit parameters from photometric data. Building on this framework, Kipping (2010) demonstrated that finite integration times particularly relevant for long-cadence observations such as those from Kepler can systematically distort transit shapes and bias derived system parameters if not properly accounted for. Machine learning classifiers, such as Gaussian Process Classifiers, can rapidly evaluate thousands of candidates and assign probabilistic planet validations by incorporating features from light curves and prior astrophysical information. These models, while effective, require cross-verification due to possible caveats and discrepancies with traditional methods (Armstrong *et al*., 2020).

False positives signals mimicking planetary transits produced by eclipsing binaries, background stars, or instrumental artifacts are a significant challenge in validation. Statistical validation tools like BLENDER utilize detailed light curve modelling to simulate blend scenarios and compare these to observations, effectively excluding false positive scenarios for candidates such as Kepler-10c. Complementary high spatial-resolution imaging with adaptive optics helps identify contaminant stars near the target that could dilute or create false transit-like signals, aiding BLENDER analyses (Adams *et al*., 2012). Another powerful validation tool, vespa, quantitatively computes false positive probabilities (FPP) for transiting candidates by considering astrophysical scenarios and stellar properties, enabling large-scale automated validation of thousands of objects including Kepler Objects of Interest (KOIs). Modern validation frameworks have evolved beyond BLENDER and vespa to handle the volume and complexity of TESS and future PLATO data. ExoMiner (and its successor ExoMiner++) is a deep learning classifier trained on Kepler and TESS vetting features that achieves >95% recall and precision on known planet catalogs (Valizadegan *et al*., 2021). Recent machine learning approaches such as ExoMiner have improved candidate validation (Yakubu *et al.,* 2025). RAVEN (Robust Automated Vetting Environment) employs a Bayesian framework to compute false-positive probabilities using pixel-level diagnostics and multi-band photometry (Hadjigeorghiou *et al*., 2025).

Dynamical Characterization via Transit Timing Variations (TTVs)

Transit Timing Variations (TTVs) arise from gravitational interactions between planets in multi-planet systems, causing deviations from strictly periodic transit times. The amplitude and period of TTVs depend on planetary masses, orbital periods, eccentricities, and mutual inclinations. The mass–eccentricity degeneracy is a well-known challenge in TTV inversion, where similar timing signals can be produced by different combinations of planetary mass and orbital eccentricity (Agol & Fabrycky, 2018). However, high-frequency TTV components arising from near-resonant interactions can break this degeneracy and yield precise mass measurements (Hadden & Lithwick, 2017).

Detection Completeness and Biases

The sensitivity of transit surveys is quantified via completeness metrics, most commonly the Combined Differential Photometric Precision (CDPP) for Kepler and TESS, which measures the photometric noise on transit timescales. Detection efficiency is assessed through injection–recovery tests, where synthetic transit signals are inserted into real light curves and pipeline detection rates are measured (Christiansen *et al*., 2020). These tests reveal strong biases against small planets ($R_p < 2\ R\oplus$), long periods ($P > 50$ days), and planets orbiting active stars. Detrending choices (e.g., spline order, filter width) significantly influence completeness: aggressive filtering can remove shallow transits, while insufficient detrending elevates false-positive rates. Systematic corrections such as CBV (Cotrending Basis Vectors) in Kepler and PCD (Presearch Data Conditioning) in TESS mitigate instrumental noise but may also attenuate astrophysical signals. Recent pipelines (e.g., DIAmante, EVEREST) employ Gaussian Process or wavelet-based detrending to preserve transit signals while removing stellar variability (Luger *et al*., 2018).

RESULTS AND DISCUSSION

Planetary Occurrence Rates and Stellar Dependencies

Completeness-corrected analyses of Kepler and TESS data now provide statistically robust occurrence rates across stellar types, planetary sizes, and orbital periods. For FGK stars, the integrated occurrence rate for planets

between 0.5–16 R⊕ and orbital periods of 1–400 days is 1.52 ± 0.08 planets per star (Dattilo *et al*., 2023). This overall rate masks significant dependencies on planetary size and stellar properties:

Size Dependence: The occurrence rate follows a steeply rising power law toward smaller planets, with $df/d\log R \propto R^{\alpha}$ and $\alpha = -1.92 \pm 0.11$ (Howard *et al*., 2011). For specific size ranges around Sun-like stars, occurrence rates are 0.130 ± 0.008, 0.023 ± 0.003, and 0.013 ± 0.002 planets per star for the 2–4, 4–8, and 8–32 R⊕ ranges, respectively (Howard *et al*., 2011).

Stellar Mass/Temperature Dependence: Occurrence rates for small planets (≈1–4 R⊕) increase dramatically with decreasing stellar mass. Planets in the 2–4 R⊕ range are approximately seven times more common around cool stars (3600–4100 K) than around the hottest stars (6600–7100 K) in the Kepler sample (Howard *et al*., 2011). This trend continues to mid-M dwarfs, where the ratio of rocky to volatile-rich planets increases substantially (Cloutier *et al*., 2019).

Habitable Zone Occurrence: For Earth-sized planets (0.75–1.5 R⊕) in the conservative habitable zone of Sun-like stars, occurrence rates remain constrained, with recent upper limits of <0.18 planets per star (Kunimoto & Matthews, 2020). Accounting for systematic uncertainties, plausible occurrence rates for such planets with periods of 237–500 days are estimated between 0.03–0.40 per FGK star (Hsu *et al*., 2019).

Table 1: Planetary Occurrence Rates

Stellar Type	Planet Size (R⊕)	Period (days)	Occurrence planets/star	Uncertainty	Primary Source
FGK	0.5–16	1–400	1.52	±0.08	Dattilo *et al*. (2023)
Sun-like	1–2	1–100	0.30	±0.07	Bryson *et al*. (2021) Kepler DR25
M dwarfs	0.5–1.5	1–10	~2.5	Factor of ~2	Hsu *et al*. (2020)
FGK	0.75–1.5 (HZ)	237–500	<0.18	Upper limit	Kunimoto & Matthews (2020)
FGK	All sizes	0.5–500	~1	–	Mulders *et al*. (2018)

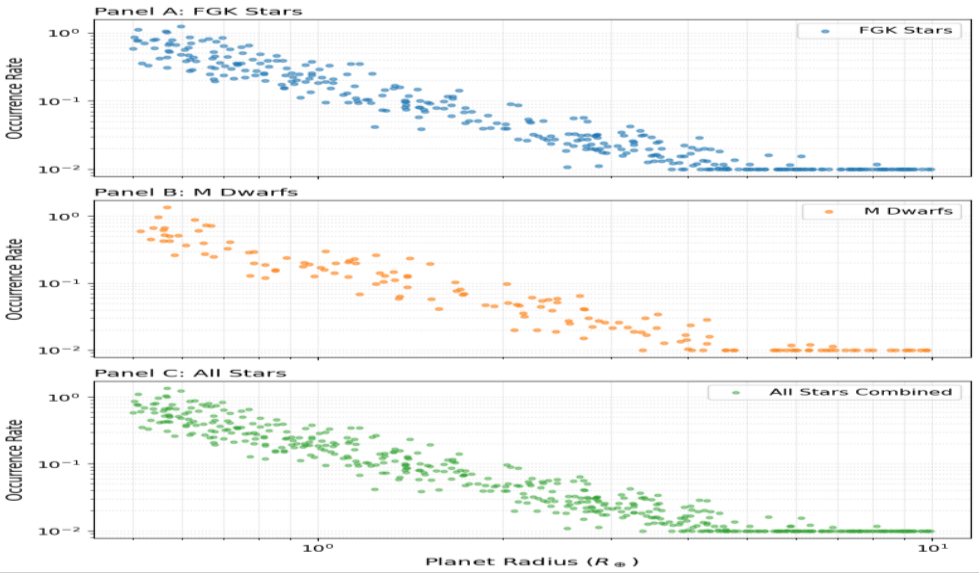

Figure 1: Illustrates the relationship between planet radius and occurrence rate for FGK stars (Panel A), M dwarfs (Panel B), and the combined stellar sample (Panel C), with both axes plotted on logarithmic scales

Overall Radius–Occurrence Trend: In all three panels, the occurrence rate decreases systematically with increasing planet radius. Small planets (≲1–2 R⊕) preferentially exhibit higher occurrence rates (typically ≳0.1), while larger planets (≳5 R⊕) cluster at lower occurrence rates (≲0.05). This inverse correlation is visually apparent across the full radius range and is consistent with a negative power-law dependence of occurrence on planet size.

Log-Log Scaling and Power-Law Behaviour: The use of logarithmic axes highlights the approximately linear alignment of the data points over much of the parameter space, indicating that a power-law model provides a reasonable description of the underlying trend. Deviations from a perfectly linear relation reflect intrinsic scatter and imposed lower limits on the occurrence rate.

Planet Radius Coverage: The planet radii span roughly 0.5–10 R⊕, corresponding to about one order of magnitude. The densest concentration of points lies below ≈3 R⊕, indicating that the synthetic sample is dominated by small planets, particularly super-Earths and sub-Neptunes.

Occurrence Rate Floor and Scatter: A noticeable accumulation of points at an occurrence rate of ≈0.01 is present in all panels, especially at larger radii. This reflects a lower cut off in the dataset and illustrates that large planets are intrinsically rarer. Substantial vertical scatter is evident at fixed radius, particularly below ≈4 R⊕, consistent with the well-known intrinsic dispersion in planet occurrence and detection completeness effects.

Comparison between Stellar Types: Panel A (FGK stars) contains a denser distribution of points than Panel B (M dwarfs), reflecting the larger fraction of FGK systems in the sample. Despite this difference in sampling density, both stellar populations exhibit a similar qualitative decline in occurrence rate with increasing planet radius. Panel C combines both samples and therefore shows the highest point density while preserving the same global trend.

The occurrence-rate trends shown in Figure 1 and Table 1 collectively indicate that planetary formation favours the production of small-radius planets, particularly around lower-mass stars. The enhanced abundance of super-Earths and sub-Neptunes around cool stars supports theoretical models in which lower stellar masses and protoplanetary disk conditions facilitate efficient formation and retention of small planetary cores. Furthermore, the decline in occurrence toward larger radii is consistent with core-accretion models predicting that giant-planet formation is intrinsically less common due to the higher solid-mass requirements and shorter disk lifetimes needed for runaway gas accretion.

The Planetary Radius Gap and Its Physical Interpretation

A cornerstone result from transit surveys is the detection of a bimodal radius distribution for small planets, known as the "radius valley" or "radius gap" (Fulton *et al*., 2017).

Empirical Characteristics:

Location: The valley minimum is observed at, R_{Valley} $1.78^{+0.14}_{-0.16}$ R⊕ for planets around FGK stars (Dattilo *et al*., 2023), separating peaks of rocky super-Earths (≈1.47 R⊕) and sub-Neptunes with volatile envelopes (≈2.72 R⊕) (Martinez *et al*., 2019).

Orbital Period Dependence: The gap's position exhibits a clear slope in radius–period space, evolving as $R_p \propto P^{-0.11}$ (Martinez *et al*., 2019), a relationship recently refined with higher precision to $R_p = P^{-0.142^{+0.006}_{-0.006}}$ (Jordan *et al*., 2025). This slope is a critical diagnostic for theoretical models.

Stellar Mass Dependence: Intriguingly, the slope of the radius gap shows an opposite trend around low-mass M dwarfs compared to Sun-like stars, suggesting stellar environment plays a key role in the underlying physical processes (Cloutier *et al*., 2019).

Theoretical Interpretation: The radius gap is a predicted signature of atmospheric mass loss over Gyr timescales. Two leading models can reproduce its observed characteristics:

1. *Photoevaporation*: High-energy X-ray and ultraviolet flux from the young star heats and strips atmospheres from planetary cores (Lopez & Fortney, 2013).
2. *Core-Powered Mass Loss*: The residual heat from a planet's formation core provides the energy to drive hydrodynamic escape (Ginzburg *et al*., 2018; Gupta & Schlichting, 2019).

The observed period dependence of the gap has been used to distinguish between these mechanisms, with recent high-precision analyses suggesting core-powered mass loss provides a better fit to the orbital period trend, while insolation flux relationships can favour photoevaporation (Jordan *et al*., 2025).

Table 2: Radius Gap Characteristics

Parameter	Value	Uncertainty / Trend	Primary Source
Valley center (FGK)	$1.78^{+0.14}_{-0.16}$ R⊕	+0.14-0.16	Fulton *et al*. (2017)
Slope (Rp ∝ P^α)	α = -0.09	±0.02	Van Eylen *et al*. (2018)
Refined slope	α = − 0.142	+0.006-0.006	Jordan et al. (2025)
M dwarf slope	Shallower/opposite	Qualitative	Cloutier & Menou (2020)
Core-powered preferred	Yes (for FGK)	Model-dependent	Gupta & Schlichting (2019)

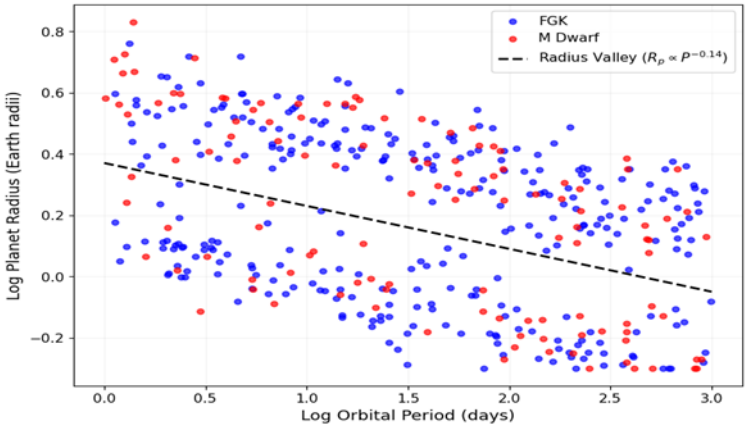

Figure 2: Shows Radius-Period Diagram

Simulated Orbital Period Range: The orbital period spans a logarithmically uniform range from 1 to 1000 days along the x-axis ($\log_{10}$ P ≈ 0–3). This range covers short-period planets through longer-period systems and is representative of the parameter space typically probed by transit surveys.

Logarithmic Scaling: Both axes are presented on logarithmic scales $\log_{10}$ (P) for orbital period and $\log_{10}$ (R_p) for planet radius. This scaling enables visualization of trends across multiple orders of magnitude and facilitates comparison with power-law relations commonly reported in exoplanet population studies.

Radius Valley Representation: A theoretical radius-valley trend is overlaid as a black dashed line, parameterized as $R_P \propto P - 0.14$, or

$log10\ (Rp) = -0.14\, log_{10}\ (P) + 0.37$

The constant offset (C = 0.37) was selected to place the valley within the bulk of the simulated planet population. This corresponds to a characteristic radius of approximately 1.7–2.0 R⊕ at periods of tens to hundreds of days, consistent with the expected location of the radius valley for FGK stars reported in observational studies (e.g. Van Eylen *et al*. 2018).

Stellar-Type Distribution: Planets orbiting FGK stars (blue points) and M dwarfs (red points) are plotted together to illustrate potential differences in their distribution relative to the radius valley. In this illustrative dataset, both populations' span similar ranges in period and radius, and no strong separation is imposed. In an observational context, one would quantitatively assess the relative planet densities above and below the valley for each stellar type to infer differences in atmospheric loss or formation pathways.

Table 3: Mass–Radius Relationships

Planet Type	Radius (R⊕)	Mass (M⊕)	Primary Source
Rocky (Earth-like)	<1.5	<6	Zeng *et al*. (2019)
Sub-Neptunes	1.5–3.5	2–20	Otegi *et al*. (2020)
Scatter below 4 R⊕	High	High	Wolfgang *et al*. (2016)

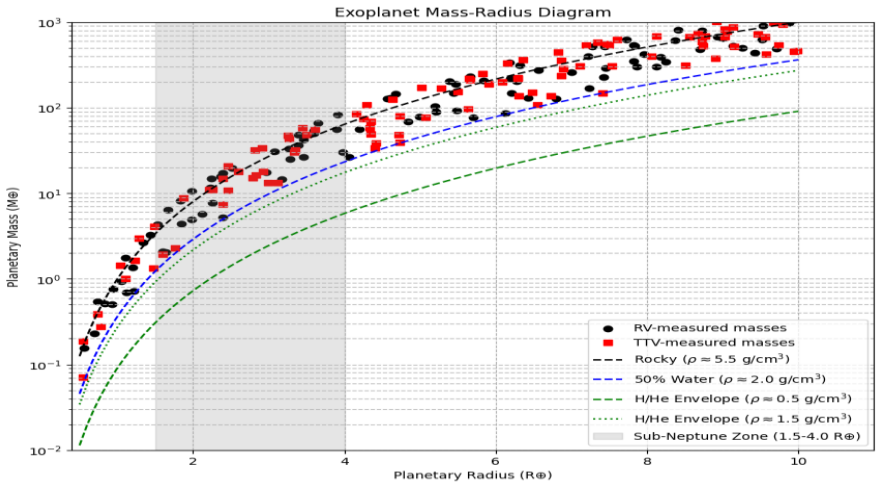

Figure 3: Exoplanet Mass-Radius Diagram

The simulated mass–radius distribution exhibits trends that closely mirror those reported in observational exoplanet surveys and theoretical studies of planetary interiors. Across the full radius range (0.5–10 R⊕), planetary mass increases with radius but with increasing dispersion toward larger sizes. This behaviour is consistent with the expectation that planetary composition, rather than size alone, increasingly governs mass beyond the purely rocky regime (Zeng *et al*. 2016; Otegi *et al*. 2020).

Planets with radii below approximately 1.5 R⊕ cluster tightly around the rocky mass–radius relation, corresponding to bulk densities near Earth-like values ($\rho \approx 5.5$ g cm^{-3}). This limited scatter suggests relatively homogeneous internal structures dominated by silicate mantles and iron cores, in agreement with observational analyses indicating that most planets below ≈1.6 R⊕ are predominantly rocky (Rogers 2015; Zeng *et al*. 2019).

In contrast, the sub-Neptune regime (≈1.5–4.0 R⊕) displays substantial dispersion in mass at fixed radius. This region is well known observationally for its compositional diversity, encompassing planets with water-rich interiors, substantial volatile layers, and varying fractions of H/He envelopes (Wolfgang *et al*. 2016; Lopez & Fortney 2014). The broad overlap between RV- and TTV-measured planets in this regime reinforces the conclusion that planets of similar radii can have markedly different masses and internal structures. Such diversity has been widely interpreted as evidence of competing formation and evolutionary processes, including envelope accretion, photo-evaporative mass loss, and core-powered mass loss (Gupta & chlichting 2019).

At radii larger than approximately 4 R⊕, the simulated planets increasingly follow low-density H/He envelope curves, consistent with gas-dominated compositions. Observational mass–radius studies similarly show that planets in this size range are best explained by substantial gaseous envelopes, with mass scaling more weakly with radius than in the rocky regime (Kipping 2017). The growing separation between rocky and envelope-dominated theoretical curves emphasizes that planetary mass in this regime is controlled primarily by atmospheric content rather than solid core size.

The observed radius valley therefore provides strong empirical evidence that atmospheric evolution plays a dominant role in shaping close-in exoplanet populations. The period dependence of the gap, together with its variation across stellar types, suggests that both stellar irradiation and intrinsic planetary thermal evolution contribute to atmospheric escape processes. Consequently, the radius gap has become a critical observational benchmark for distinguishing between photoevaporation and core-powered mass-loss models.

Atmospheric Characterization with JWST

The James Webb Space Telescope (JWST) has revolutionized transmission spectroscopy, enabling precise molecular detections in exoplanet atmospheres. Early results include the unambiguous detection of CO_2, H_2O, SO_2, and CH_4 in the atmosphere of the hot Saturn WASP-39 b (Alderson *et al*., 2023), and constraints on atmospheric metallicity, C/O ratios, and cloud properties across diverse planet populations. Practical metrics such as the Transmission Spectroscopy Metric (TSM) and Emission Spectroscopy Metric (ESM) are used to prioritize targets for JWST follow-up (Kempton *et al*., 2018). However, stellar contamination (e.g., unocculted spots, faculae) and limb-darkening biases remain significant challenges, introducing wavelength-dependent offsets that can mimic or obscure atmospheric features (Rackham *et al*., 2024). Differentiable atmospheric retrieval frameworks (e.g., Pyrat Bay, petitRADTRANS) now incorporate flexible limb-darkening models and stellar activity corrections to mitigate these systematics.

These early JWST observations demonstrate that transmission spectroscopy has entered a precision era in which atmospheric composition, cloud structure, and chemical disequilibrium can be constrained simultaneously. The improved sensitivity of JWST not only validates previous HST-based detections but also enables the characterization of smaller and cooler planets, thereby extending comparative exoplanetology beyond hot Jupiters toward potentially habitable terrestrial worlds.

Discussion

Transit photometry has fundamentally reshaped our understanding of exoplanetary demographics, system architectures, and evolutionary pathways. The detection of the radius valley an observed bimodality in the size distribution of small planets provides compelling evidence for atmospheric mass-loss processes operating over Gyr timescales (Fulton *et al*., 2017; Martinez *et al*., 2019). The observed slope of the valley in radius–period space, particularly its dependence on stellar type, supports core-powered mass loss as a dominant mechanism for FGK stars while suggesting that photoevaporation or other processes may prevail around M dwarfs (Cloutier *et al*., 2019; Jordan *et al*., 2025). These findings not only constrain planetary evolution models but also inform the interpretation of occurrence rates, which reveal that small planets are significantly more common around low-mass stars (Howard *et al*., 2011; Dattilo *et al*., 2023). The prevalence of compact, multi-planet systems exhibiting "peas-in-a-pod" architectures further indicates that planet formation often proceeds in a relatively quiescent, dynamically cold environment, leading to intra-system uniformity in size and spacing (Millholland *et al*., 2017).

Despite its success, transit photometry remains subject to significant biases and limitations. Geometric constraints restrict detection to systems with nearly edge-on orbits, while stellar activity and instrumental noise can mimic or obscure transit signals (Deeg & Alonso, 2018). Advances in validation frameworks such as vespa, TRICERATOPS, and deep-learning classifiers like ExoMiner have mitigated false positives but underscore the need for multi-wavelength and high-resolution follow-up (Valizadegan *et al*., 2021). Looking ahead, synergies with radial velocity, astrometry, and especially transmission spectroscopy with JWST will enable more complete characterization of planetary masses, atmospheres, and bulk compositions (Alderson *et al*., 2023; Rackham *et al*., 2024).

CONCLUSION

Transit photometry stands as the most prolific method for exoplanet discovery and characterization, having unveiled thousands of planets and enabled statistical studies of their properties. From revealing the radius gap and diverse system architectures to facilitating atmospheric spectroscopy with JWST, this technique continues to drive explanatory science forward. Future missions such as PLATO and the Habitable Worlds Observatory will build on this legacy by targeting Earth-sized planets in habitable zones and deepening our understanding of planet formation and potential habitability.

As data volumes continue to increase, the integration of artificial intelligence and machine-learning techniques into transit detection, candidate validation, light-curve detrending, and atmospheric retrieval will become increasingly important for handling next-generation survey datasets efficiently and accurately. Machine-learning frameworks such as ExoMiner already demonstrate the potential of AI-assisted validation in reducing false positives and accelerating exoplanet discovery. Consequently, the combined application of advanced computational methods, photo dynamical modelling, and multi-method observational follow-up will ensure that transit photometry remains central to the exploration and characterization of planetary systems beyond the Solar System.

REFERENCES

Adams, E., Ciardi, D., Dupree, A., Iii, T., Kulesa, C., & Mccarthy, D. (2012). Adaptive Optics Images of Kepler Objects of Interest. https://doi.org/10.48550/arxiv.1205.5535

Agol, E., and Fabrycky, D. C. (2018). Transit-timing and duration variations for the discovery and characterization of exoplanets. In Handbook of exoplanets (pp. 797-816). *Springer*, Cham.

Akash Gupta, Hilke E Schlichting, Sculpting the valley in the radius distribution of small exoplanets as a by-product of planet formation: the core-powered mass-loss mechanism, *Monthly Notices of the Royal Astronomical Society*, Volume 487, Issue 1, July 2019, Pages 24–33, https://doi.org/10.1093/mnras/stz1230

Alderson, L., Wakeford, H.R., Alam, M.K. et al. Early Release Science of the exoplanet WASP-39b with JWST NIRSpec G395H. *Nature* 614, 664–669 (2023). https://doi.org/10.1038/s41586-022-05591-3

Armstrong, D. J., Gamper, J., & Damoulas, T. (2020). Exoplanet validation with machine learning: 50 new validated Kepler planets. *Monthly Notices of the Royal Astronomical Society*, 504(4), 5327–5344. https://doi.org/10.1093/mnras/staa2498

Babu, G. J. (2018). Statistical Challenges in Exoplanet Detection. 1–10. https://doi.org/10.1002/9781118445112.stat07939

Barclay, T., Quintana, E. V., & Pepper, J. (2018). A Revised Exoplanet Yield from the Transiting Exoplanet Survey Satellite (TESS). *The Astrophysical Journal Supplement Series,* 239(1), 2. https://doi.org/10.3847/1538-4365/aae3e9

Barnes, J. W. (2007). Effects of orbital eccentricity on extrasolar planet transit detectability and light curves. Publications of the Astronomical Society of the Pacific, 119(859), 986–993. https://doi.org/10.1086/522039. ArXiv: 0708.0243

Brown, T., & Latham, D. (2008). Expected Planet and False Positive Detection Rates for the Transiting Exoplanet Survey Satellite. https://doi.org/10.48550/arxiv.0812.1305

Bryson, S., Coughlin, J., Batalha, N. M., Berger, T., Huber, D., Burke, C., and Mullally, S. E. (2020). A probabilistic approach to Kepler completeness and reliability for exoplanet occurrence rates. *The Astronomical Journal*, 159(6), 279.

Bryson, S., Kunimoto, M., Kopparapu, R. K., Coughlin, J. L., Borucki, W. J., Koch, D.,.. & Zamudio, K. A. (2020). The occurrence of rocky habitable-zone planets around solar-like stars from Kepler data. *The Astronomical Journal*, 161(1), 36.

Burleigh, M. (2017). The Next Generation Transit Survey. *Proceedings of the International Astronomical Union*, 14(S339), 22. https://doi.org/10.1017/s1743921318002132

Burt, J., & Barclay, T. (2017). Getting Ready for TESS: an On-hand Software Tutorial. Proceedings of the *International Astronomical Union*, 14(S339), 220–225. https://doi.org/10.1017/s1743921318002648

Burt, J., Zellem, R., Ciardi, D., Kanodia, S., Bryden, G., Kataria, T., Pearson, K., Christiansen, J., Beichman, C., Fulton, B., & Swain, M. (2025). A New Approach to Compiling Exo-atmospheric Target Lists and Quantifying the Ground-Based Resources Needed to Vet Them. https://doi.org/10.48550/arxiv.2508.03801

Butler, R. P., Wright, J. T., Marcy, G. W., Fischer, D. A., Vogt, S. S., Tinney, C. G., Jones, H. R. A., Carter, B. D., Johnson, J. A., McCarthy, C., & Penny, A. J. (2006). Catalog of nearby exoplanets. The Astrophysical Journal, 646(1), 505–522. https://doi.org/10.1086/504701

Cassan, A. (2021). New Worlds Ahead: The Discovery of Exoplanets (pp. 121–147). *Springer*. https://doi.org/10.1007/978-3-030-67392-5_4

Catala, C., & Consortium, T. P. (2008). PLATO: PLAnetary Transits and Oscillations of stars. *Journal of Physics*: *Conference Series*, 118(1), 012040. https://doi.org/10.1088/1742-6596/118/1/012040

Chen, J., & Kipping, D. (2017). Probabilistic forecasting of the masses and radii of other worlds. *The Astrophysical Journal,* 834(1), 17. https://doi.org/10.3847/1538-4357/834/1/17

Christiansen, J. L., Clarke, B. D., Burke, C. J., Jenkins, J. M., Bryson, S. T., Coughlin, J. L., ... & Campbell, J. (2020). Measuring transit signal recovery in the Kepler pipeline. IV. Completeness of the DR25 planet candidate catalog. *The Astronomical Journal*, 160(4), 159.

Claret, A. (2000). A new non-linear limb-darkening law for LTE stellar atmosphere models. Calculations for −5.0 ≤ log [M/H] ≤ +1, 2000 K ≤ Teff ≤ 50000 K at several surface gravities. Astronomy & Astrophysics, 363, 1081–1190.

Cloutier, R., & Menou, K. (2020). Evolution of the radius valley around low-mass stars from Kepler and K2. *The Astronomical Journal*, 159(5), 211. https://doi.org/10.3847/1538-3881/ab8237

Coulombe, L.-P., Roy, P.-A., & Benneke, B. (2024). Biases in Exoplanet Transmission Spectra Introduced by Limb-darkening Parametrization. *The Astronomical Journal*, 168(5), 227. https://doi.org/10.3847/1538-3881/ad7aef

Cowley, M., & Hughes, S. (2014). Characterization of transiting exoplanets by way of differential photometry. *Physics Education*, 49(3), 293–298. https://doi.org/10.1088/0031-9120/49/3/293

Dattilo, A., Batalha, N. M., & Bryson, S. (2023). A unified treatment of kepler occurrence to trace planet evolution. I. Methodology. *The Astronomical Journal*, 166(3), 122.

Deeg, H., & Alonso, R. (2018). Transit Photometry as an Exoplanet Discovery Method. https://doi.org/10.48550/arxiv.1803.07867

Fulton, B. J., Petigura, E. A., Howard, A. W., Isaacson, H., Marcy, G. W., Cargile, P. A., Hebb, L., Weiss, L. M., Johnson, J. A., Morton, T. D., Sinukoff, E., Crossfield, I. J. M., & Hirsch, L. A. (2017). The California-Kepler Survey. III. A gap in the radius distribution of small planets. *The Astronomical Journal*, 154(3), 109. https://doi.org/10.3847/1538-3881/aa80eb

Ginzburg, S., Schlichting, H. E., & Sari, R. E. (2018). Core-powered mass-loss and the radius distribution of small exoplanets. *Monthly Notices of the Royal Astronomical Societ*y, 476(1), 759-765.

Hadden, S., & Lithwick, Y. (2017). Kepler planet masses and eccentricities from TTV analysis. *The Astronomical Journal,* 154(1), 5. https://doi.org/10.3847/1538-3881/aa71ef

Hadjigeorghiou, A., Armstrong, D. J., Cui, K., Magro, M. L., Nieto, L. A., Díaz, R. F., & Kunovac, V. (2025). RAVEN: Ranking and Validation of Exoplanets. *arXiv preprint arXiv:*2509.17645.

Heller, R., Hippke, M., & Rodenbeck, K. (2019). Transit least-squares survey. *Astronomy and Astrophysics*, 625, A31. https://doi.org/10.1051/0004-6361/201935276

Howard, A. W., Marcy, G. W., Bryson, S. T., Jenkins, J. M., Rowe, J. F., Batalha, N. M., & MacQueen, P. J. (2012). Planet occurrence within 0.25 AU of solar-type stars from Kepler. *The Astrophysical Journal Supplement Series*, 201(2), 15.

Hsu, D. C., Ford, E. B., Ragozzine, D., & Ashby, K. (2019). Occurrence rates of planets orbiting FGK stars: Combining Kepler DR25, Gaia DR2, and Bayesian inference. *The Astronomical Journal,* 158(3), 109.

Irwin, J., Hebb, L., Aigrain, S., Moraux, E., Hodgkin, S., & Irwin, M. (2007). The Monitor project: data processing and light curve production. *Monthly Notices of the Royal Astronomical Society*, 375(4), 1449–1462. https://doi.org/10.1111/j.1365-2966.2006.11408.x

Jiang, J., Ji, X., Cowan, N., Hu, R., & Zhu, Z. (2019). Empirical Predictions for the Period Distribution of Planets to be discovered by the Transiting Exoplanet Survey Satellite. https://doi.org/10.48550/arxiv.1906.06795

Jordan, D., & Song, I. (2025). Precise Parameters from Bayesian Spectral Energy Distribution Fitting Indicate Thermally Driven Mass Loss Likely Driver of Radius Valley. *The Astronomical Journal,* 169(5), 234.

Kempton, E. M. R., Bean, J. L., Louie, D. R., Deming, D., Koll, D. D., Mansfield, M., & von Essen, C. (2018). A framework for prioritizing the TESS planetary candidates' most amenable to atmospheric characterization. *Publications of the Astronomical Society of the Pacific*, 130(993), 114401.

Kipping, D. M. (2010). Binning is sinning: morphological light-curve distortions due to finite integration time. *Monthly Notices of the Royal Astronomical Society*, 408(3), 1758-1769.

Kunimoto, M., & Matthews, J. M. (2020). Searching the entirety of Kepler data. II. Occurrence rate estimates for FGK stars. *The Astronomical Journal*, 159(6), 248.

Lopez, E. D., & Fortney, J. J. (2014). Understanding the mass–radius relation for sub-Neptunes: radius as a proxy for composition. The Astrophysical Journal, 792(1), 1.

Luger, R., Agol, E., Kruse, E., Barnes, R., Becker, A., Foreman-Mackey, D., & Deming, D. (2018). EVEREST: Tools for de-trending stellar photometry. *Astrophysics Source Code Library*. Ascl: 1807.029

Macdougall, M. G., Fulton, B., Blunt, S., Tyler, D., Kosiarek, M., Giacalone, S., Holcomb, R., Batalha, N. M., Robertson, P., Polanski, A. S., Dalba, P. A., Lubin, J., Akana Murphy, J. M., Hill, M. L., Van Zandt, J., Scarsdale, N., Gilbert, G. J., Pidhorodetska, D., Chontos, A., & Turtelboom, E. V. (2023). The TESS-Keck Survey. XV. Precise Properties of 108 TESS Planets and Their Host Stars. *The Astronomical Journal*, 166(1), 33. https://doi.org/10.3847/1538-3881/acd557

Mandel, K., & Agol, E. (2002). Analytic light curves for planetary transit searches. *The Astrophysical Journal,* 580(2), L171.

Martinez, C. F., Cunha, K., Ghezzi, L., & Smith, V. V. (2019). A spectroscopic analysis of the California-Kepler survey sample. I. Stellar parameters, planetary radii, and a slope in the radius gap. *The Astrophysical Journal*, 875(1), 29.

Mills, S. M., & Mazeh, T. (2017). The Planetary Mass–Radius Relation and Its Dependence on Orbital Period as Measured by Transit Timing Variations and Radial Velocities. *The Astrophysical Journal Letters*, 839(1), L8.

Mohr, J. J., Bertin, E., Tucker, D., Gruendl, R., Swanson, M., Yanny, B., Armstrong, R., Marriner, J., Hanlon, W., Gower, M., Daues, G., Sevilla, I., Petravic, D., Lin, H., Tomashek, T., Desai, S., & Kuropatkin, N. (2012). The Dark Energy Survey data processing and calibration system. 8451, 84510D. https://doi.org/10.1117/12.926785

Mulders, G. D., Pascucci, I., Apai, D., & Ciesla, F. J. (2018). The exoplanet population observation simulator. I. The inner edges of planetary systems. *The Astronomical Journal*, 156(1), 24.

Osborn, H., Armstrong, D., Brown, D., Mccormac, J., Doyle, A., Louden, T., Kirk, J., Spake, J., Lam, K.,

Walker, S., Faedi, F., & Pollacco, D. (2015). Single Transit Candidates from K2: Detection and Period Estimation. https://doi.org/10.48550/arxiv.1512.03722

Otegi, J. F., Dorn, C., Helled, R., *et al*. (2020) — Impact of the measured parameters of exoplanets on the inferred internal structure, *Astronomy and Astrophysics*, 640, A135

Pál, A., Kiss, C., & Molnár, L. (2018). TESS in the Solar System. Publications of the Astronomical Society of the Pacific, 130(993), 114503. https://doi.org/10.1088/1538-3873/aae2aa

Perryman, M. (2012). The History of Exoplanet Detection. Astrobiology, 12(10), 928–939. https://doi.org/10.1089/ast.2011.0784

Rackham, B. V., & de-Wit, J. (2024). Toward Robust Corrections for Stellar Contamination in JWST Exoplanet Transmission Spectra. *The Astronomical Journal*, 168(2), 82.

Rogers, L. A. (2015). Most 1.6 Earth-radius planets are not rocky. *The Astrophysical Journal,* 801(1),

Seager, S., & Mallén-Ornelas, G. (2003). A unique solution of planet and star parameters from an extrasolar planet transit light curve. The Astrophysical Journal, 585(2), 1038–1055. https://doi.org/10.1086/346105

Valizadegan, H., Martinho, M., Wilkens, L. S., Jenkins, J. M., Smith, J., Caldwell, D. A., Twicken, J. D., Gerum, P. C., Walia, N., Hausknecht, K., Lubin, N. Y., Bryson, S. T., & Oza, N. C. (2021). ExoMiner: A highly accurate and explainable deep learning classifier that validates 301 new exoplanets. *arXiv*. https://doi.org/10.48550/arXiv.2111.10009

Van Eylen, Camilla Agentoft, M S Lundkvist, H Kjeldsen, J E Owen, B J Fulton, E Petigura, & Snellen, I. (2018). An asteroseismic view of the radius valley: stripped cores, not born rocky, *Monthly Notices of the Royal Astronomical Society,* Volume 479, Issue 4, Pages 4786–4795, https://doi.org/10.1093/mnras/sty1783

Volker Springel. 2010. Smoothed Particle Hydrodynamics in Astrophysics. Annual Review Astronomy and Astrophysics. 48:391-430. https://doi.org/10.1146/annurev-astro-081309-130914

Vwavware, J. O., Mu'allim, Y., Ohwofosirai, A., & Ojobeagu, O. A. (2025). The Impact of Robotic Telescopes on Time-Domain Astronomy. *Nigerian Journal of Applied Physics*, 1(1), 1-9.

Weiss, L. M., & Marcy, G. W. (2014). The mass–radius relation for 65 exoplanets smaller than 4 Earth radii. The Astrophysical Journal Letters, 783(1), L6. https://doi.org/10.1088/2041-8205/783/1/L6

Winn, J. (2007). Precise Photometry and Spectroscopy of Transits. https://doi.org/10.48550/arxiv.0710.1098

Wolfgang, A., Rogers, L. A., & Ford, E. B. (2016). Probabilistic mass–radius relationship for sub-Neptune-sized planets. *The Astrophysical Journal*, 825(1), 19.

Yakubu, M., Iheanyichukwu, C. A., & Anderson, K. A. (2023). The Study of the Photometry and Flare Analysis of Kepler Flare Candidate 2MASS J22285440-1325178. *American Journal of Astronomy and Astrophysics,* 10(2), 14-22.

Yakubu, M., Vwavware, J. O., Adrian, O., & Ogheneovo, A. (2025). Machine Learning Applications in Exoplanet Detecion: From KEPLER to TESS. *FUDMA Journal of Sciences*, 9(7), 215-221. https://doi.org/10.33003/fjs-2025-0907-3478

Yang, C. (2024). Analysis and Comparison of Three Exoplanet Searching Schemes. Highlights in Science, Engineering and Technology, 88, 914–921. https://doi.org/10.54097/hdw3ng92

Zeng, L., Jacobsen, S. B., Sasselov, D. D., Petaev, M. I., Vanderburg, A., Lopez-Morales, M., ... & Wordsworth, R. D. (2019). Growth model interpretation of planet size distribution. *Proceedings of the National Academy of Sciences*, 116(20), 9723-9728.

Zeng, L., Sasselov, D. D., & Jacobsen, S. B. (2016). Mass–radius relation for rocky planets based on PREM. The Astrophysical Journal, 819(2), 127.